*Scientia Iranica*, Vol. 13, No. 2, pp 124–133


SCIENTIA
IRANICA

# Large Eddy Simulation of Separated Flow over a Wall-Mounted Cube

**M. Farhadi[1] and M. Rahnama[*]**

Large eddy simulation of flow over a wall-mounted cube in a channel was performed at a Reynolds number of 40000. The structure function modeling of the subgrid-scale stress terms was used with three slightly varying versions of its selective type. The convective terms were discretized using a QUICK scheme, along with a relatively coarse grid. A series of time-averaged velocities and turbulent stresses were computed and compared with experimental data to examine the performance of these models. The structure function model yielded deficient mean flow structure and turbulence statistics compared with the selective structure function. While none of these models could reproduce experimental results exactly, the results of time-averaged streamline plots and turbulent kinetic energy for one of the selective structure function models showed less discrepancy with experimental data compared with other models. It was shown that implementation of a wall function does not improve the results considerably and, in general, with a coarse grid resolution, it is possible to obtain some reasonable results as compared to the experiment.

## INTRODUCTION

Turbulent flow past three-dimensional bluff bodies has attracted much attention because of the wide range of engineering applications, such as electronic boards and the flow around tall buildings. Accurate prediction of flow characteristics is required in such applications to be sure of a safe and economical design. Numerical simulation of flow in such configurations is capable of revealing detailed information, which is much more necessary than its experimental counterpart.

A wall-mounted cube subjected to the flow in a channel is a basic geometry (Figure 1) with some important phenomena, such as flow separation with partial reattachment, wake flow periodicity and large-scale turbulence structures. There is a vast amount of literature about experiments undertaken for this geometry [1-6]; among them being the comprehensive work of Martinuzzi and Tropea [5] for a Reynolds number of 40000. Their flow picture given in Figures 2a and 3a shows the very complex flow nature, in spite of its simple geometry. As observed in these figures, the flow separates in front of the cube; in the mean there is a primary separation vortex and, also, a secondary one, while, instantaneously, up to three separation vortices were detected. The main vortex bends as a horseshoe vortex around the cube into the wake; having a typical converging-diverging behavior. The flow separates at the front corners of the cube on the roof and sidewalls. In the mean, it does not

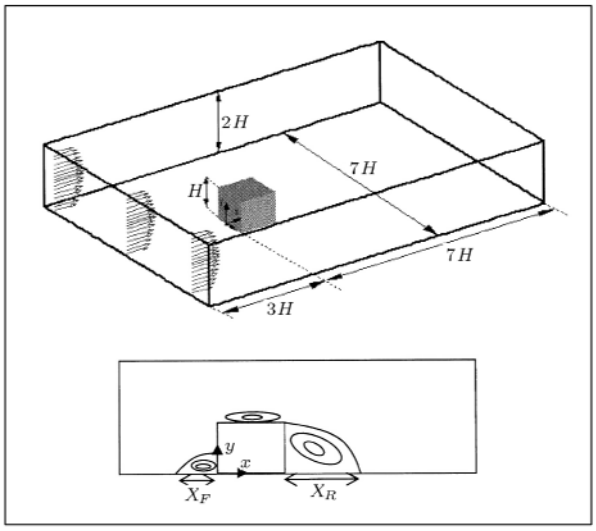


**Figure 1.** Geometry of computational domain and schematic of recirculation zones.

1. *Department of Mechanical Engineering, Shahid Bahonar University of Kerman, Kerman, I.R. Iran.*
*. *Corresponding Author, Department of Mechanical Engineering, Shahid Bahonar University of Kerman, Kerman, I.R. Iran.*

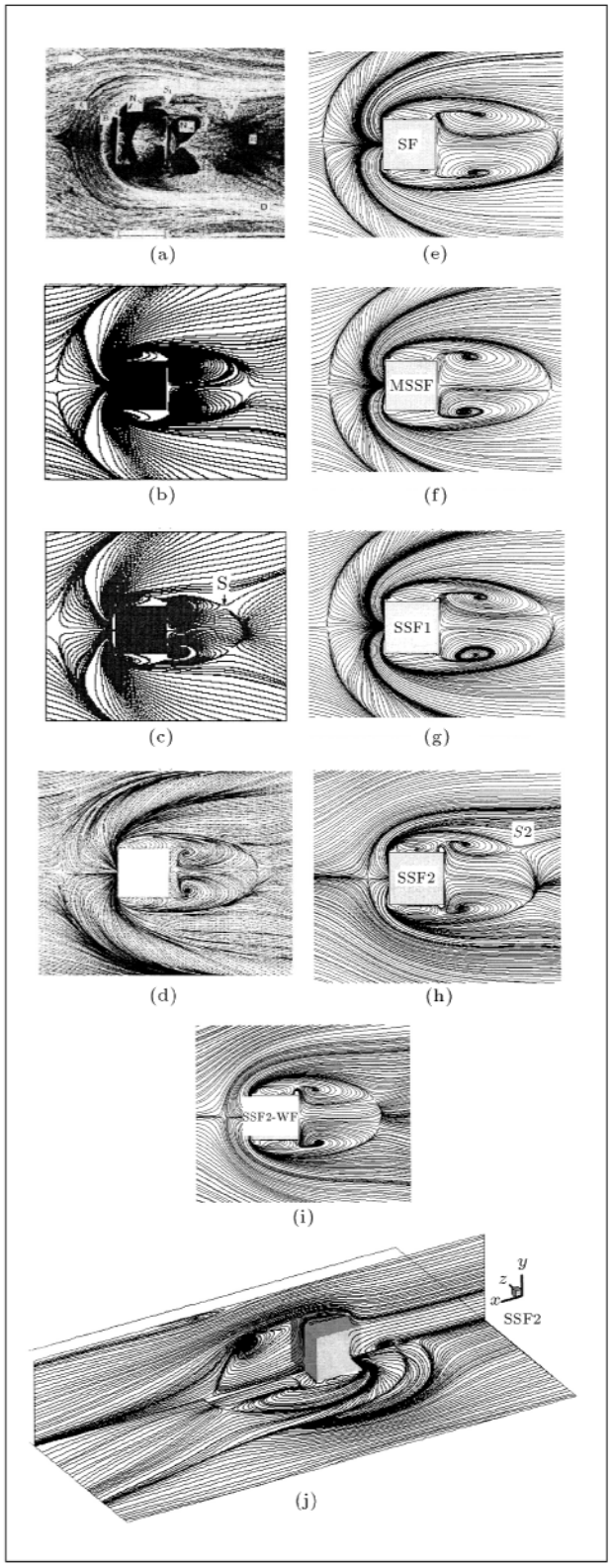


**Figure 2.** Time-averaged computations of streamline plots at the floor of the channel by (a) Experiments [5], (b) OEM model [10], (c) LDKM model [10], (d) Computations of Shah and Ferziger [9], (e) SF model, (f) MSSF model, (g) SSF1 model, (h) SSF2 model, (i) SSF2-WF model, all at Re = 40000 and (j) SSF2 model at Re = 3200.

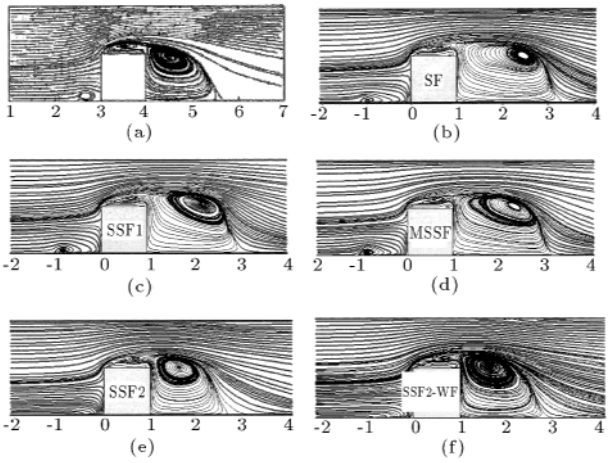


**Figure 3.** Comparison of time-average streamline plots at plane $z = 0$ obtained from (a) Experimental data and (b-f) Present computations.

reattach on the roof. A large separation region develops behind the cube that interacts with the horseshoe vortex. Numerical investigation of such complex flow configuration is a challenge for researchers in the field of computational fluid mechanics.

Various authors have done numerical predictions of turbulent flow over a wall-mounted cube in a channel using Direct Numerical Simulation (DNS), Large Eddy Simulation (LES), Reynolds-Averaged Navier-Stockes equations (RANS) [7] and, recently, Detached Eddy Simulation (DES) [8]. In fact, several international workshops have been held on this flow configuration [7]. The two Reynolds numbers used in these computations were 3000 and 40000. These workshops indicated that LES is able to predict the main characteristics of such flow configuration more accurately than RANS and much more cheaply than DNS computations. The subgrid-scale models used in these computations were Smagorinsky, dynamic and mixed models. Many of these LES computations used a fine grid resolution (more than $10^6$ nodes for low Reynolds number). Shah and Ferziger [9] reported LES simulation of flow around a cubic obstacle at Re = 40000 with $192 \times 64 \times 96$ grid points. Using no wall function for the region near the wall, these simulations approach Direct Numerical Simulation (DNS), resolve the near-wall streaks and may be described as Quasi-DNS (QDNS) [10]. In such circumstances, the influence of the Subgrid-Scale (SGS) model is then small. Although these LES were carried out with considerable success, the extension of this kind of simulation to a higher Reynolds number and more complex geometry implies very high computational costs.

Recently, Iaccarino et al. [11] studied the accuracy of unsteady RANS turbulent models in predicting flow around a square cylinder and over a surface-mounted cube that is located in a channel with a 3-cube-height

in a spanwise direction. Their simulations were done with a $v^2 \quad f$ turbulence model. Results showed that an improved prediction of reattachment lengths and vortex shedding could be obtained with unsteady RANS calculations at the expense of higher computational time, compared to the steady RANS calculation of Rodi [12]. It was mentioned that steady computations produce an erroneously long wake, because they omit an important component of the averaged flow field, i.e., the periodic vortex shedding.

The most recent published work in this flow configuration is that of Kranjovic and Davidson [10,13] who have published calculations for an LES simulation of flow over a surface-mounted cube for Re = 40000. They reported the results of their two computations: A dynamic one-equation subgrid-scale model and one with no SGS model. They used a coarse grid for their computations with a low resolution near the wall. However, as compared with the results obtained from a high near-wall resolution, a good correspondence was observed. Their results of time-averaged streamwise velocity showed a good correspondence with experimental data, but, they observed a poor agreement for other components of the velocity. The Reynolds stresses computed with their model showed much better predictions than those without an SGS model, as compared to the experiment. They argued that improved results with a coarse grid could be obtained, because of the more accurate equation dynamic model proposed by Davidson [14].

There is an extensive body of work on flow over a cube mounted inside a channel. However, computations could be performed using new types of subgrid-scale stress tensor modeling to evaluate their performance. Murakami [15] reported the results of applying new models and new methods of LES in the computation of flow over bluff bodies. One of those models, which has not been applied to this geometry, is the Structure Function model (SF) [16,17]. This model, based on the eddy viscosity hypothesis, uses the local kinetic energy spectrum. As the SF model was too dissipative for two-dimensional vortices, the Selective Structure Function (SSF) model was proposed, in which three-dimensional effects could be much better implemented than SF [17]. Various authors used SF and SSF for different flow configuration, such as a backward facing step, a bluff rectangular plate and, recently, a wall-mounted cube [17-19].

In the present study, SF and SSF models of LES were used for computation of turbulent flow over a wall-mounted cube. As the number of grid points plays an important role in lessening the computational time and cost of LES, the authors directed their attention toward investigating the effect of coarse grid resolution in the present computation. They evaluated this by using both different versions of SSF and wall function implementation in a near-wall region. The results were then compared with previous published works and experimental data.

## MATHEMATICAL FORMULATION AND COMPUTATIONAL DETAILS

### Mathematical Model

Turbulent flow over bluff bodies may be modeled by LES, where the larger three-dimensional unsteady turbulent motions are directly represented, while the effect of small scales of motion is modeled. To do this, a filtering operation is introduced to decompose the velocity vector ($u_i$) into the sum of a filtered (or resolved) component, $\overline{u}_i$, and a residual (or subgrid-scale) component, $u_i'$. This operation can be represented with a filter of width $\Delta x$, such that convolution of any quantity $f(x_i,t)$ by the filter function $G_{\Delta x}(x_i)$ is in the following form:

$$\overline{f}(x_i,t) = \int f(y_i,t)G_{\Delta x}(x_i \quad y_i)dy_i, \quad f' = f \quad \overline{f}. \tag{1}$$

The equations for the evolution of the filtered velocity filed are derived from Navier-Stokes equations. These equations are of the standard form, with the momentum equation containing the residual stress tensor. The application of the filtering operation to the continuity and Navier-Stokes equations gives the resolved Navier-Stokes equations, which, in non-dimensional incompressible form, are as follows:

$$\frac{\partial \overline{u}_i}{\partial x_i} = 0, \tag{2}$$

$$\frac{\partial \overline{u}_i}{\partial t} + \frac{\partial}{\partial x_j}(\overline{u}_i\overline{u}_j) = \quad \frac{\partial \overline{P}}{\partial x_i} + \frac{1}{\mathrm{Re}}\nabla^2\overline{u}_i \quad \frac{\partial \tau_{ij}}{\partial x_j}, \tag{3}$$

where $\overline{P}$ is the pressure, $\overline{u}_1$, $\overline{u}_2$ and $\overline{u}_3$ are the streamwise, cross-stream and spanwise component of velocity, respectively, which govern the dynamics of the large, energy-carrying scales of motion. The Reynolds number is defined as $U_{\mathrm{mean}}H/\upsilon$, where $U_{\mathrm{mean}}$ and $H$ are the average velocity of the entrance profile and cube height, respectively. The effect of small scales upon the resolved part of the turbulence appears in the Subgrid Scale (SGS) stress term, $\tau_{ij} = \overline{u_iu_j} \quad \overline{u}_i\overline{u}_j$, which must be modeled.

The main effect of the subgrid-scale stresses is dissipative, i.e. it withdraws energy from the part of the spectrum that can be resolved. One model for subgrid-scale stress term $\tau_{ij}$ is based on its dependence on the filtered strain rate through an eddy-viscosity:

$$\tau_{ij} = \upsilon_t\left(\frac{\partial \overline{u}_i}{\partial x_j} + \frac{\partial \overline{u}_j}{\partial x_i}\right) + \frac{1}{3}\tau_{kk}\delta_{ij}. \tag{4}$$

In this study, the eddy viscosity ($\upsilon_t$) is evaluated using Subgrid-Scale (SGS), Structure Function (SF) and Selective Structure Function (SSF) models. In the Structure Function model, the eddy-viscosity is evaluated according to Lesier and Métais [16]:

$$\upsilon_t^{\mathrm{SF}}(\mathbf{x},\Delta c,t) = 0.105 {C_k}^{3/2} \Delta c \sqrt{F_2(\mathbf{x},\Delta c,t)}, \qquad (5)$$

where $\Delta c = (\Delta x_1 \times \Delta x_2 \times \Delta x_3)^{\frac{1}{3}}$ is the geometric mean of the meshes in the three spatial directions. $C_k$ is the Kolmogrov constant and $F_2$ is the local structure function constructed with the filtered velocity field $\overline{\mathbf{u}}(\mathbf{x},t)$:

$$F_2(\mathbf{x},\Delta c,t) = \frac{1}{6}\sum_{i=1}^{3}\Big\langle [\overline{\mathbf{u}}(\mathbf{x},t) \quad \overline{\mathbf{u}}(\mathbf{x}+\Delta x_i,t)]^2 + [\overline{\mathbf{u}}(\mathbf{x},t) \quad \overline{\mathbf{u}}(\mathbf{x} \quad \Delta x_i,t)]^2 \Big\rangle \left(\frac{\Delta c}{\Delta x_i}\right)^{\frac{2}{3}}, \qquad (6)$$

$F_2$ is calculated with a local statistical average of square (filtered) velocity differences between $\mathbf{x}$ and the six closest points surrounding $\mathbf{x}$ on the computational grid. In some cases, the average may be taken over four points parallel to a given plane.

In the selective version of the Structure Function model, the eddy-viscosity is switched off in the regions where the flow is not enough three-dimensionally. The three-dimensional criterion is as the following: One measures the angle ($\alpha$) between the vorticity at a given grid point and the average vorticity at the six closest neighboring points (or the four closest points in the four-point formulation). If this angle were less than 20°, the most probable value, according to simulations of isotropic turbulence at the resolution of $32^3$ $64^3$, the eddy viscosity would be canceled and only molecular dissipation would act. In this situation, the flow is locally close to a two-dimensional state. As compared to the original SF model, this subgrid-scale model dissipates the resolved scale energy at fewer points of the computational domain, as compared to the SF model. The model constant of 0.105 (see Equation 5) has then to be increased to satisfy energy conservation. It is calculated by requiring the eddy viscosity, given by the SSF model averaged over the entire computational domain to equal the corresponding one obtained with the SF model. One finds that the constant in Equation 5 has to be multiplied by 1.56 [17].

$$\upsilon_t^{\mathrm{SSF}}(\mathbf{x},\Delta c,t) = 0.1638 \Phi_{20^\circ}(\mathbf{x},t) {C_K}^{3/2} \Delta c [F_2(\mathbf{x},\Delta c,t)]^{1/2}, \qquad (7)$$

where $\Phi_{20^\circ}(\mathbf{x},t)$ is the indicating function based on the value of ($\alpha$):

$$\Phi_{20^\circ}(\mathbf{x},t) = \begin{cases} 1 & \text{if} \quad \alpha \geq 20^\circ \\ 0 & \text{if} \quad \alpha < 20^\circ \end{cases} \qquad (8)$$

The results of computations using Equation 7 are called SSF1 in this paper. Suksangpanomrung et al. [18] used a smoothly varying function rather than an abrupt cut-off, $\Phi'_{20^\circ}(\mathbf{x},t)$ instead of $\Phi_{20^\circ}(\mathbf{x},t)$, which is evaluated using a smoothly varying function, defined as:

$$\Phi'_{20^\circ}(\mathbf{x},t) = \begin{cases} 0 & \text{for} \quad \alpha < 10^\circ \\ e^{\ (\frac{d\alpha}{3^\circ})^2} & \text{for} \quad 20^\circ \geq \alpha \geq 10^\circ \\ & \text{and} \quad d\alpha = |\alpha \quad 20^\circ| \\ 1 & \text{for} \quad \alpha > 20^\circ \end{cases} \qquad (9)$$

In Equation 9, all angles are in radian. This method was used by Suksangpanomrung et al. [18] for separated flow over a bluff rectangular plate and the results were in good agreement with experimental data. This model was used in the present computation with results mentioned in the name of SSF2.

Recently, Ackermann and Métais [20] proposed a modified version of the Selective Structure Function model. They argued that the Modified Selective Structure Function model (MSSF) respects, in a better way, the energetic exchanges between the resolved and subgrid scales, as compared to the Selective Structure Function model (SSF) and automatically adjusts itself to the discretization thinness of the most energetic scales. In the model of MSSF, the eddy viscosity is computed from:

$$\upsilon_t^{\mathrm{MSSF}}(\mathbf{x},\Delta c,t) = C_{\mathrm{MSSF}} \Phi_{\alpha_c}(\mathbf{x},t) {C_K}^{3/2} \Delta c [F_2(\mathbf{x},\Delta c,t)]^{1/2}, \qquad (10)$$

where $C_{\mathrm{MSSF}}$ is a constant very close to 0.142 and $\Phi_{\alpha_c}(\mathbf{x},t)$ is given by:

$$\Phi_{\alpha_c}(\mathbf{x},t) = \begin{cases} 1 & \text{if} \quad \alpha > \alpha_c \\ 0 & \text{if} \quad \alpha < \alpha_c \end{cases} \qquad (11)$$

$\alpha_c$ is the critical angle, which is a function of the ratio of cut-off wave-number, $K_c$, to the wave-number $K_i$, $K_c/K_i$, at which the spectrum peaks (see Ackermann and Métais [20]). It was shown that if $\alpha_c$ were taken as equal to 20°, the classical SSF model, Equation 7, would be obtained with a reduced constant of 0.142 instead of 0.1638. Therefore, for computations of MSSF, Equation 9 is used with a change of constant from 0.1638 to 0.142.

## Numerical Method

The governing equations presented in the preceding section were discretized using a finite volume method with a staggered grid. The convective terms were discretized using a QUICK scheme. The QUICK scheme has some deficiencies, such as large numerical dissipation, as compared with the Central Difference

(CD) scheme. However, it was already used in a LES simulation of flow over a wall-mounted cube [7], especially in LES computations using no subgrid-scale model. An important issue in LES computations is that of using, at least, a second order accuracy of both time and spatial discretization of the equations. On the other hand, the CD has the shortcoming of producing an oscillatory solution in the coarse grid computation. As the primary objective of the present computations was to select one of the three versions of the SSF model on a coarse grid, the QUICK scheme was used in these computations.

The convective and diffusive fluxes in the momentum and energy equations were treated explicitly in the present computations. A third order Runge-Kutta algorithm is used for the time integration in conjunction with the classical correction method at each sub-step. The continuity Equation 1 and the pressure gradient term in the momentum Equation 2 are treated implicitly, while the convective and diffusive terms are treated explicitly. This method, called a semi-implicit fractional step, provides an approach that does not use pressure in the predictor step as in the pressure corrector method (such as the well-known SIMPLE family of algorithms). The linear system of pressure is solved by an efficient conjugate gradient method with preconditioning. Further details on the numerical method are given in Suksangpanomrung [21].

## Computational Domain and Boundary Condition

The computational domain consists of a plane channel with a cubic obstacle of dimension ($H$) mounted on one of its walls (Figure 1). Channel height is selected as $2H$, due to the available experimental data that were reported for a cube with a half channel height dimension [7]. The spanwise width of the channel was selected as $7H$, such that the cube is located in the middle with an equal distance from the spanwise boundaries of $3H$. The upstream distance from the front side of the cube to the inlet boundary was selected as $3H$ and the downstream distance was $6H$. These selected dimensions were based on the previous published works mentioned in [7,9,10,12,13].

The boundary conditions used in the present calculations are as follows: The inlet boundary condition was selected as a fully developed turbulent velocity distribution (one-seventh power law). It is noteworthy that this inlet boundary condition does not exactly correspond to that of the experiments. However, comparison of velocity profile and Reynolds stress at the upstream of the cube ($x/H = 1.0$) shows negligible discrepancies with experiments for the SSF2 model, as observed in Figure 4. In other words, the difference between the experimental inlet velocity profile and the one used in the present computations of the SSF2 model, diminishes upstream of the cube. The outlet boundary condition is of a convective type with $U_c$ equal to the mean velocity, as follows:

$$\frac{\partial u_1}{\partial t} + U_c \frac{\partial u_1}{\partial x_1} = 0. \tag{12}$$

Obviously, such a convective boundary condition is capable of predicting unsteady flow behavior at the exit with good accuracy. The spanwise boundary condition was selected as periodic. The minimum grid spacing used in the present computations is 0.03 in all three dimensions adjacent to the cube surface with a grid expansion ratio of 1.05. Using a no-slip boundary condition with such a grid resolution near the wall may raise the question of accuracy. To answer this question, the computations were performed with a wall function calculation [22]. The results showed a negligible difference in predicted velocity components near the wall. The number of grid points used in the present computation was $113 \times 51 \times 100$ in the $x$-, $y$- and $z$-direction, respectively. This was based on the computations of Krajnovic and Davidson [10]. They used three different grid point distributions: $82 \times 50 \times 66$, $162 \times 66 \times 98$ and $210 \times 66 \times 114$ and compared the mean reattachment lengths upstream

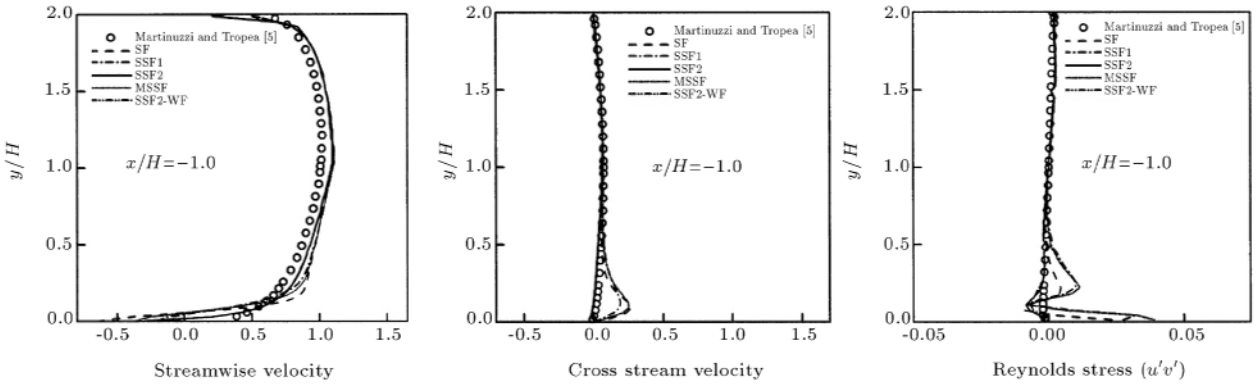


**Figure 4.** Time-averaged streamwise, cross stream and Reynolds stress profiles at plane $z = 0$ and $x/H = 1.0$.

and downstream of the cube, $X_F$ and $X_R$, respectively, with the experiment. The percentage of error in $82 \times 50 \times 66$ grid points was 6.73 for $X_F$ and 14.28 for $X_R$, which reduced to 5.77 and 9.75, respectively, for $210 \times 66 \times 114$ grid points. Such a decrease in error is not economical when there is an increase of more than a million grid points, which increases computational time drastically. They also reported that very small differences between the mean velocity profiles were observed using the medium and fine grid. As both SF models and the one-equation model of Krajnovic and Davidson [10] are based on the spectral kinetic energy of turbulence, it seems that the same reasoning could be used for the present computations. The CFL (Courant-Friedrichs-Lewy) number is less than one for all computations with the maximum value of 0.95. The average time in the simulation was $200H/U_{\text{mean}}$, where $H$ is the cube height and $U_{\text{mean}}$ is the bulk velocity at the inlet.

## RESULTS

Results are presented in the form of time-averaged quantities, including streamline plots, velocity components, Reynolds stress and turbulent kinetic energy. The present computations were done for Re=40000, for which the experiments are available, namely, flow visualization studies and the detailed LDA measurements of Martinuzzi and Tropea [5]. They obtained the flow pictures given in Figures 2a and 3a, which show clearly the very complex nature of the flow in spite of its simple geometry. Figures 2 and 3 show the streamlines in the near channel floor and plane of symmetry, respectively, for different models used in the present calculations. All of them show a horseshoe vortex around the cube and the separation regions on the roof, lateral sides and behind the cube. The main point about horseshoe vortex is its converging-diverging behavior in the experimental measurement. This phenomenon has not been observed in most of the previous computations (see Figures 2b, 2c and 2d), especially for Re = 40000 [9,10]. In the present work, such behavior was not predicted for most of the subgrid-scale models used except for the SSF2 model (see Figure 2h). Such behavior could be observed at a lower Reynolds number. Our computation for Re=3200 shows clearly this converging-diverging behavior of the horseshoe vortex (see Figure 2j).

The size and shape of the horseshoe vortex is clearly shown in Figure 2. As discussed by Martinuzzi and Tropea [5] (Figure 2a), two recirculation regions exist upstream of the cube. All calculations predicted the primary recirculation with its center located at $X_R$. No author has detected the secondary recirculation zone, which is very small and close to the front side of cube, through numerical computation. In the lateral side of the cube, there are two saddle points, observed in the experiment (Figure 2a, points $S_1$ and $S_2$) and separated by a distance. While most computations detected the point $S_1$, a limited number of them could predict the point $S_2$ (Figure 2c). In the present computations, point $S_2$ could be detected by the SSF2 model shown in Figure 2h. Computations obtained with other models in the present study could not show clearly the location of these points.

Figure 3 shows different recirculation zones at plane $z = 0$. Three recirculation zones are observed clearly, both in the experiment and in the present computations. The most accurate results, concerning the downstream recirculation zone, are related to the SSF2 model computation that is observed in Figure 3e. The size and central location of the downstream recirculation zone obtained from SF, SSF1 and MSSF models have some differences with the experiment. This may be due to the coarse grid resolution used in the present computations. Table 1 compares various lengths of separation regions defined in Figure 1. It is observed that none of the models used can predict both upstream and

**Table 1.** Reattachment lengths, $X_R$ and $X_F$ (Figure 1), obtained from models and experiment.

| Contribution | Number of Grids | Minimum Grid Spacing | $X_F$ | $X_R$ |
|---|---|---|---|---|
| Martinuzzi and Tropea (Exp.) [5] | ——— | ——— | 1.04 | 1.61 |
| Hussein and Martinuzzi (Exp.) [6] | ——— | ——— | 1.04 | 1.67 |
| SF model | $113 \times 51 \times 100$ | 0.03 | 1.11 | 2.25 |
| SSF1 model | $113 \times 51 \times 100$ | 0.03 | 1.036 | 2.05 |
| MSSF model | $113 \times 51 \times 100$ | 0.03 | 1.067 | 2.13 |
| SSF2 model | $113 \times 51 \times 100$ | 0.03 | 0.4 | 1.62 |
| SSF2 model (with Wall Function, WF) | $113 \times 51 \times 100$ | 0.03 | 0.59 | 1.71 |
| OEM model [10] | $82 \times 50 \times 66$ | 0.023 | 0.97 | 1.380 |
| LDKM model [10] | $82 \times 50 \times 66$ | 0.023 | 0.944 | 1.413 |
| Shah and Ferziger [9] | $192 \times 64 \times 96$ | 0.006 | 1.050 | 1.650 |

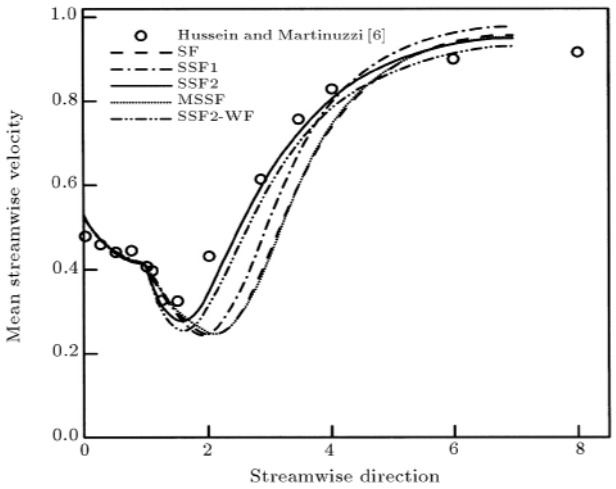


**Figure 5.** Variation of time-averaged mean streamwise velocity at plane $z = 0$.

downstream recirculation lengths correctly. The SSF2 model predicts downstream reattachment length in reasonable agreement with experimental data, except for the location of its center, but, its value, obtained for the upstream recirculation length, is too short. It should be mentioned that computations performed by SSF2 with a wall function could improve upstream recirculation length slightly. Other models predict the upstream recirculation length close to the experimental one, but, poor correspondence with experimental results were observed for the downstream recirculation length.

Mean streamwise velocity, integrated in a $y$-direction at the plane $z = 0$, is plotted in Figure 5 for the various models used and compared with experimental data. All computations follow the trend of experimental data. Among various models used in the present computations, SSF2 shows better agreement with the experiment, especially in the downstream recirculation region ($1.5 < x < 4.0$). The effect of inserting a wall function in the SSF2 computation is observed in this figure, which shows a negligible decrease in mean streamwise velocity as compared to the SSF2 model.

A series of time-averaged resolved velocities and turbulent stresses are computed and compared with the experiments in Figure 6. The locations are selected from $x/H = 0.5$ to 4.0 at $z = 0.0$. Results obtained for locations upstream of the cube were not shown, because no significant flow feature exists in that region except for a small recirculation region. The computed mean velocity for this region showed good correspondence with the experiment, in spite of the differences that exist in the upstream recirculation length computed, as mentioned in the preceding discussion. While streamwise velocity distribution near the top surface of the cube at $x/H = 0.5$ shows discrepancies with the experimental data of $u$ $w$ plane measurements, its behavior, for most of the region between the top side of the cube and the channel wall, are in reasonable agreement with the experiment. The main reason for such a prediction is the quantitative difference between the experiment and the present computations of the recirculation region above the cube, which, in turn, could be a result of low grid resolution and the QUICK scheme used for the discretization of convective terms. Among the four turbulence models used in the present computations, again, SSF2 shows better agreement with experimental data at $x/H = 2.0$. Figure 6, also, shows the cross-stream velocity distribution. Shah and Ferziger [9] explained that the quality of computational results deteriorate for a vertical velocity component, as compared to the experimental data. Computations of Krajnovic and Davidson [10] showed considerable discrepancies in the vertical velocity component as compared to the experiment. As observed in Figure 6, the authors' computations for a cross-stream velocity component show good correspondence with the experimental data, especially those obtained from the SSF2 model. Another parameter of interest in this flow is the Reynolds stresses. Prediction of the $\overline{u'v'}$ profile reveals that all models predict the trend of experimental results with some discrepancies, except at $x/H = 1.0$ for the SSF2 model. Displacement of the predicted minimum value of $\overline{u'v'}$, as compared to the experiment, is due to the different flow fields obtained, as mentioned before. As grid resolution and the discretization scheme is the same for all models, the question may arise as to why there are differences in the predicted results. The reason for such behavior is the type of switching-off of the eddy viscosity in the three SSF models. As there is a continuous energy cascade from large to small eddies, the subgrid-scale model used should reveal this behavior. The MSSF and SSF1 models, which use a cut-off function for removing turbulent eddy viscosity, produce acceptable results when a fine grid resolution is used. As a coarse-grid resolution was used in the present calculations, it is expected that these two models would not be able to produce acceptable results. The SSF2 model uses a continuous type of function for switching-off the turbulent eddy viscosity (see Equation 9) and, therefore, could perform better in a coarse grid resolution. So, results obtained from SSF2 are more reliable than those from SSF1 and MSSF.

Deficiency in the predicted turbulent kinetic energy variation over the cube is observed in Figure 6. Discrepancies reduce when moving toward the end point of the upper side of the cube. This is because of a smaller and thinner separation region as compared to the experiment, which implies that excessively large turbulent diffusion should be created in this region. The profile of the computed turbulent kinetic energy for $x/H = 2.0$ and 2.5 follows the trend of the exper-

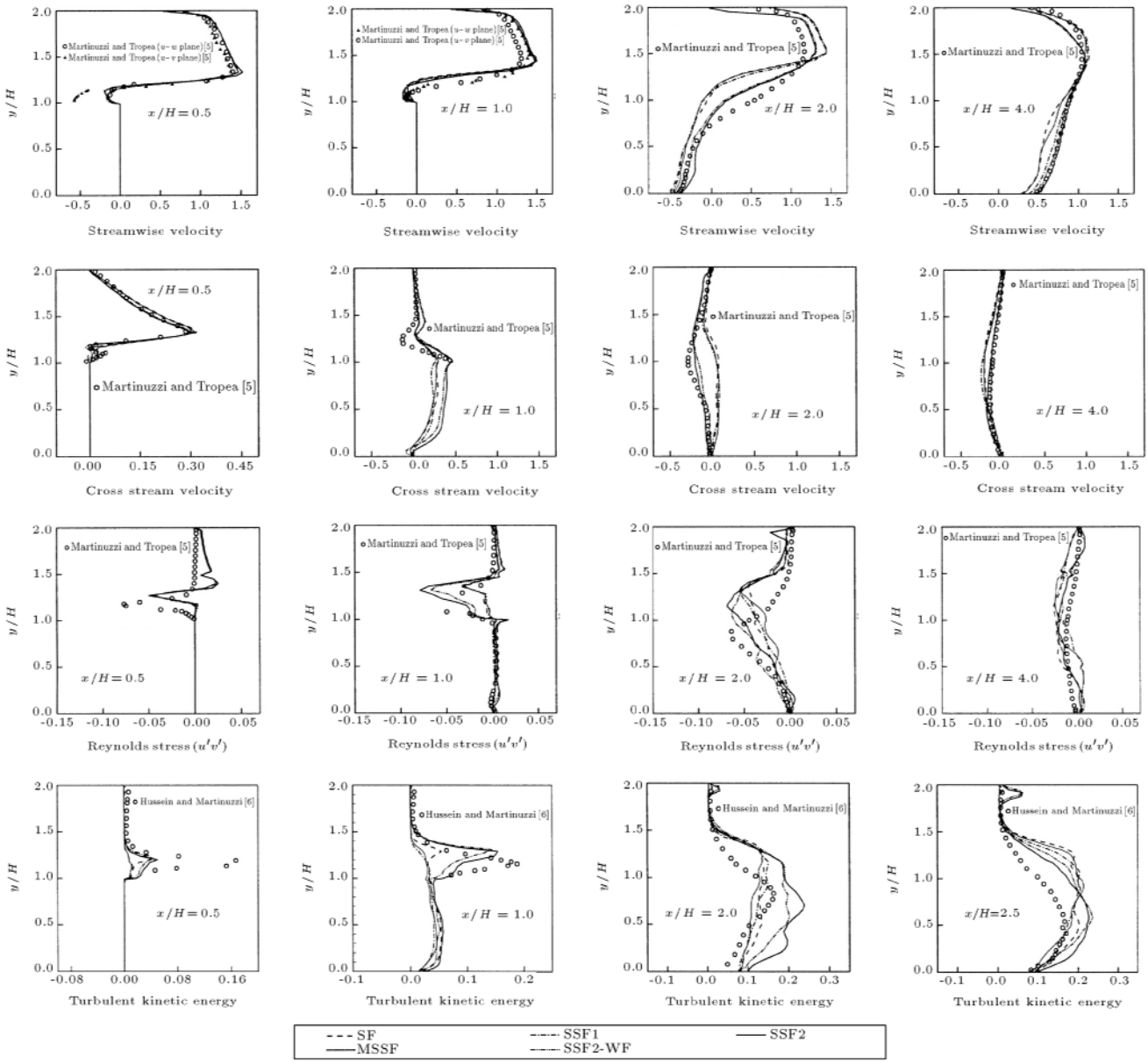


**Figure 6.** Time-averaged streamwise, cross-stream, Reynolds stress and turbulent kinetic energy profiles compared with experimental data at Re = 40000.

iment, with their values higher than the experimental ones. It is expected that less discrepancies occur between the present computation and the experiment for $x/H > 2.5$, but, no experimental data were available for $x/H > 2.5$. Here, it is observed that the SSF2 model is able to predict results closer to the experiment than other models, especially at the leading edge of the cube.

One of the complex phenomena in the flow over a cube in a channel is the formation of vortices and their subsequent stretching. Using vorticity isosurfaces for such phenomena is not suitable, as this method does not clearly distinguish the vortex near the cube. In order to identify the flow structures more clearly, the technique of 5[23] was used in the present work. In this method, the vortex cores are obtained from instantaneous velocity fields. The vortex cores are identified with a region of negative $\lambda_2$, which is the second largest eigenvalue of the tensor, $S_{ik}S_{kj} + \Omega_{ik}\Omega_{kj}$. The definitions of $S_{ij}$ and $\Omega_{ij}$, which are the symmetric and anti-symmetric parts of the velocity gradient tensor ($u_{i,j} = \frac{\partial u_i}{\partial x_j}$), are as follows:

$$S_{ij} = (u_{i,j} + u_{j,i})/2, \tag{13}$$

$$\Omega_{ij} = (u_{i,j} \quad u_{j,i})/2. \tag{14}$$

The isosurfaces of the second largest eigenvalue ($\lambda_2$) were plotted in Figure 7. Figures 7a to 7f show

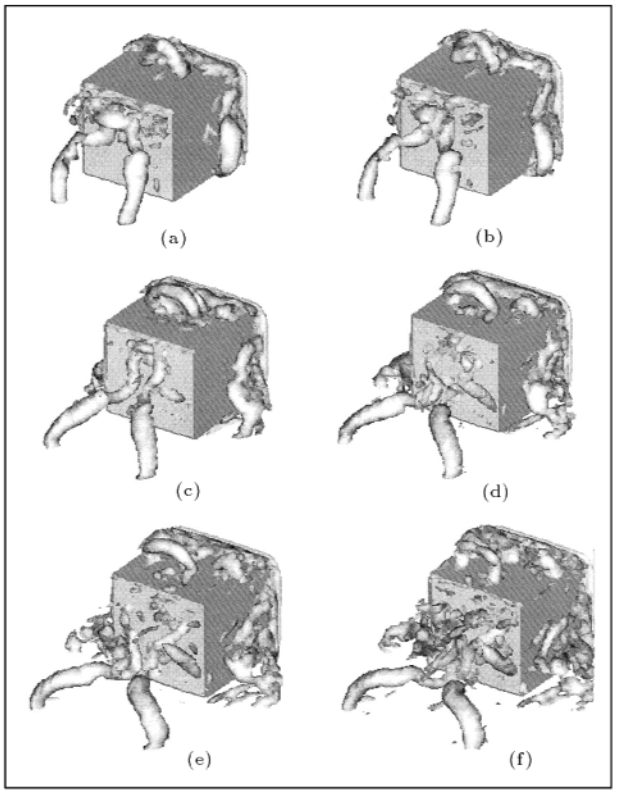


**Figure 7.** Instantaneous isosurfaces of second invariant of the velocity gradient $Q = 2500$ with the time difference between the two pictures of $tU_{\text{mean}}/H = 0.2$ (view of the back face of the body (SSF2 model)).

the formation of a vortex in the top, side and back faces of the cube surface, along with its stretching and breakdown into small eddies.

## CONCLUSION

Flow around a wall-mounted cube in a channel was computed using a Structure Function and three slightly varying versions of Selective Structure Function models at Re = 40000. A relatively coarse grid resolution with a minimum grid spacing of 0.03H was used in the present calculations. It was observed that, in general, the results obtained from Selective Structure Function modeling followed the trend of the experimental data better than those of the Structure Function. Among the three versions of the Selective Structure Function models used, the one with a smoothly varying function (SSF2) was able to reproduce results in better agreement with the experiment than the others. This is due to the continuous type of the function used in switching-off the turbulent eddy viscosity, which performs better in a coarse grid resolution as compared with SSF1 and MSSF models. Modified Selective Structure Function modeling [20] could not predict better results than those of the SSF1 model for this geometry in such a coarse grid. Using a type of wall function in the present computations showed negligible improvement in the results as compared with those obtained from computations with no wall function.

## NOMENCLATURE

| | |
|---|---|
| $C_k$ | Kolmogorov constant |
| $E(K)$ | kinetic energy spectrum |
| $G_{\Delta x}(x_i)$ | filter function |
| $H$ | cube height |
| $K_c$ | cut-off wavenumber |
| $P$ | pressure |
| Re | Reynolds number based on the height of the cube, $U_{\text{mean}}H/\upsilon$ |
| $t$ | time step |
| $\mathbf{u}$ | velocity vector |
| $U_c$ | convective mean velocity |
| $u_i$ | instantaneous velocity components |
| $U_{\text{mean}}$ | average velocity at the entrance |
| $\mathbf{x}$ | position vector |
| $x_i$ | Cartesian coordinate, $x_1, x_2, x_3$ |
| $\alpha$ | angle |
| $\upsilon$ | kinematic viscosity |
| $v_t^{\text{SF}}$ | turbulent eddy-viscosity obtained from SF |
| $\Delta$ | minimum grid spacing |
| $\tau_{ij}$ | subgrid scale (SGS) stress tensor |
| $\Delta x_i$ | grid spacing |
| $\Phi_{20^\circ}$ | indicating function, Equation 8 |

## REFERENCES

1. Castro, I.P. and Robins, A.G. "The flow around surface-mounted cube in uniform and turbulent streams", *J. of Fluid Mech.*, **79**(2), pp 307-335 (1977).
2. Castro, I.P.J. "Measurements in shear layers separating from surface-mounted bluff bodies", *J. of Wind Eng. and Ind. Aerodynamics*, **7**, pp 253-272 (1981).
3. Schofield, W. and Logan, E. "Turbulent shear flow over surface-mounted obstacles", *ASME J. of Fluids Eng.*, **112**, pp 376-385 (1990).
4. Larousse, A., Martinuzzi, R. and Tropea, C. "Flow around surface-mounted, three-dimensional obstacles", *9th Int. Sym. on Turbulent Shear Flow*, Springer-Verlag, pp 127-139 (1991).
5. Martinuzzi, R. and Tropea, C. "The flow around surface-mounted prismatic obstacles placed in a fully developed channel flow", *ASME J. of Fluids Eng.*, **115**, pp 85-92 (1993).
6. Hussein, H.J. and Martinuzzi, R.J. "Energy balance for turbulent flow around a surface mounted cube placed in a channel", *Phys. of Fluids*, **8**, pp 764-780 (1996).

7. Rodi, W., Ferziger, J.H., Breuer, M. and Pourquie, M. "Workshop on LES of flows past bluff bodies", *Rotach-Egern*, Germany (June 1995).
8. Schmidt, S. and Thiele, F. "Comparison of numerical methods applied to the flow over wall-mounted cube", *Int. J. of Heat and Fluid Flows*, **23**, pp 330-339 (2002).
9. Shah, K.B. and Ferziger, J.H. "A fluid mechanicals view of wind engineering: Large eddy simulation of flow past a cubic obstacle", *J. of Wind Eng. and Ind. Aerodynamics*, **67** & **68**, pp 211-224 (1997).
10. Krajnovic, S. and Davidson, L. "Large eddy simulation of the flow around a bluff body", *AIAA Journal*, **40**(5), pp 927-936 (2002).
11. Iaccarino, G., Ooi, A., Durbin, P.A. and Behnia, M. "Reynolds averaged simulation of unsteady separated flow", *Int. J. Heat Fluid Flow*, **24**, pp 147-156 (2003).
12. Rodi, W. "Comparison of LES and RANS calculations of the flow around bluff bodies", *J. of Wind Eng. and Ind. Aerodynamics*, **69**, pp 55-75 (1997).
13. Krajnovic, S. and Davidson, L. "A mixed one-equation subgrid model for large-eddy simulation", *Int. J. Heat Fluid Flow*, **23**, pp 413-425 (2002).
14. Davidson, L. "Large eddy simulation: A dynamic one-equation subgrid model for three-dimensional Recirculating flow", *11th Int. Symp. on Turbulent Shear Flow*, **3**, pp 26.1-26.6 (1997).
15. Murakami, S. "Overview of turbulent models applied in CWE-1997", *J. of Wind Eng. and Ind. Aerodynamics*, **74-76**, pp 55-75 (1998).
16. Métais, O. and Lesieur, M. "Spectral large eddy simulations of isotropic and stably-startified turbulence", *J. of Fluid Mech.*, **239**, pp 157-194 (1992).
17. Lesieur, M. and Métais, O. "New trends in LES of turbulence", *Ann. Rev. of Fluid Mech.*, **28**, pp 45-82 (1996).
18. Suksangpanomrung, A., Djilali, N. and Moinat, P. "Large eddy simulation of separated flow over a bluff rectangular plate", *Int. J. of Heat and Fluid Flow*, **21**, pp 655-663 (2000).
19. Rahnama, M. and Farhadi, M. "Large eddy simulation of flow over a wall-mounted cube", *Proc. of 12th Annual Conf. of Computational Fluid Dynamics*, Ottawa, Canada, pp 708-714 (2004).
20. Ackermann, C. and Métais, O. "A modified selective structure function subgrid-scale model", *J. of Turbulence*, **2**, pp 011 (2001).
21. Suksangpanomrung, A. "Investigation of unsteady separated flow and heat transfer using direct and large-eddy simulations", PhD Thesis, Department of Mech. Eng. University of Victoria, Victoria, USA (1999).
22. Mason, P.J. and Callen, N.S. "On the magnitude of the subgrid-scale eddy coefficient in large eddy simulations of turbulent channel flow", *J. of Fluid Mech.*, **162**, pp 439-462 (1986).
23. Jeong, J. and Hussein, F. "On the identification of a vortex", *J. of Fluid. Mech.*, **285**, pp 69-94 (1995).